PNAS
www.pnas.org

Supplementary Information for

Wafer-recyclable, environment-friendly transfer printing for large-scale thin-film nanoelectronics

Dae Seung Wie[a,1], Yue Zhang[b,1], Min Ku Kim[a], Bongjoong Kim[a], Sangwook Park[c], Young-Joon Kim[d], Pedro P. Irazoqui[d,e,f], Xiaolin Zheng[c], Baoxing Xu[b,2], Chi Hwan Lee[a,e,f,2]

[a]School of Mechanical Engineering, Purdue University, West Lafayette, IN 47907; [b]Department of Mechanical and Aerospace Engineering, University of Virginia, Charlottesville, VA 22903; [c]Department of Mechanical Engineering, Stanford University, Stanford, CA 94305; [d]School of Electrical and Computer Engineering, Purdue University, West Lafayette, IN 47907 [e]Center for Implantable Devices, Purdue University, West Lafayette, IN 47907 [f]Weldon School of Biomedical Engineering, Purdue University, West Lafayette, IN 47907

[1]D.S.W. and Y.Z. contributed equally to this work.

[2]To whom correspondence may be addressed. Email: bx4c@virginia.edu or lee2270@purdue.edu.

This PDF file includes:

Supplementary Figure Legends
Figs. S1 to S20

Other supplementary materials for this manuscript include the following:

Supplementary Movie Legends
Movies S1 to S3

www.pnas.org/cgi/doi/10.1073/pnas.1806640115

SI Appendix Figure Captions

Fig. S1. SEM images of various kinds of nanomaterials used as model systems in this report, including Si NM (top left), MoS_2 monolayer (top right), Si NRs (bottom left), and Ag NW (bottom right). The scale bars are 60 μm, 150 μm, 160 μm, and 12 μm, respectively.

Fig. S2. Representative microscope images (scale bars: 400 μm) of the thin film nanoelectronics after the debonding process.

Fig. S3. Optical images (scale bar: 2.5 cm) of a SiO_2/Si wafer that is recycled multiple times after the transfer printing processes.

Fig. S4. Optical images (scale bar: 2.5 cm) of a representative thin film nanoelectronics transferred from their fabrication SiO_2/Si wafer onto the surface of a building window (A) and covered with a commercial sticker to conceal the electronics (B).

Fig. S5. Optical images (scale bar: 1.8 cm) of a donor SiO_2/Si wafer (A) and a receiver thermally releasable tape (B) after the interfacial debonding process under dry air condition. The magnified views (scale bar: 350 μm) appear in the images on the bottom frame.

Fig. S6. A magnified view (scale bar: 1.5 cm) of a testbed sample placed in the loading stage of a custom-modified mechanical peeling apparatus used in this study.

Fig. S7. Experimental data of peeling strength as a function of peeling distance in water for varied peeling angles from 30º to 120º (A) and Ni thicknesses from 30 nm to 2.4 μm (B).

Fig. S8. Experimental data of steady-state peeling strength as a function of peeling rate in water.

Fig. S9. FEA results of maximum principle strain distribution in thin films at peeling distance of 1, 6, and 11 mm in water (A) and dry air conditions (B).

Fig. S10. FEA results of maximum principle strain distribution in thin films at peeling distance of 1, 6, and 11 mm in water for varied Ni thicknesses from 30 nm to 2.4 μm.

Fig. S11. (A) An optical image (scale bar: 8 mm) of a testbed sample that includes residues of materials after the interfacial debonding process in dry air condition. (B) The corresponding peeling strength-peeling distance curve.

Fig. S12. The corresponding linear and logarithmic scale of the transfer curves in Fig. 3B.

Fig. S13. Circuit diagrams of AND (left), OR (middle), and NOT (right) logic gates.

Fig. S14. The corresponding I-V and transfer curves to the n-MOSFETs in Fig. 4E.

Fig. S15. Calibration curves (A) and measured temperatures (B) for Si NRs-based p-i-n diode and control IR sensor.

Fig. S16. Raman spectra of as-prepared MoS_2 monolayer.

Fig. S17. Cross sectional schematic illustration of the hybrid photodiode that is comprised of Si NM and MoS_2 monolayer.

Fig. S18. Characterizations of a control hybrid photodiode built on a SiO_2/Si wafer.

Fig. S19. FEA results of maximum principle strain distribution for the hybrid photodiode at peeling distance of 1, 6, and 11 mm in water.

Fig. S20. Schematic illustrations of bend deformation (A) and the corresponding moment-curvature relation for a peeling process of thin films (B).

SI Appendix Movies

Movie S1. An experimental demonstration showing the interfacial debonding of a 4-inch wafer-size of thin film nanoelectronics in a water bath at room temperature.

Movie S2. An experimental demonstration showing the interfacial debonding process by using a custom-modified peeling apparatus.

Movie S3. An experimental demonstration displaying letters and images on a LED screen in a pre-programmed manner by exploiting the transferred Si NM-based MOSFETs-based switches on the side wall.

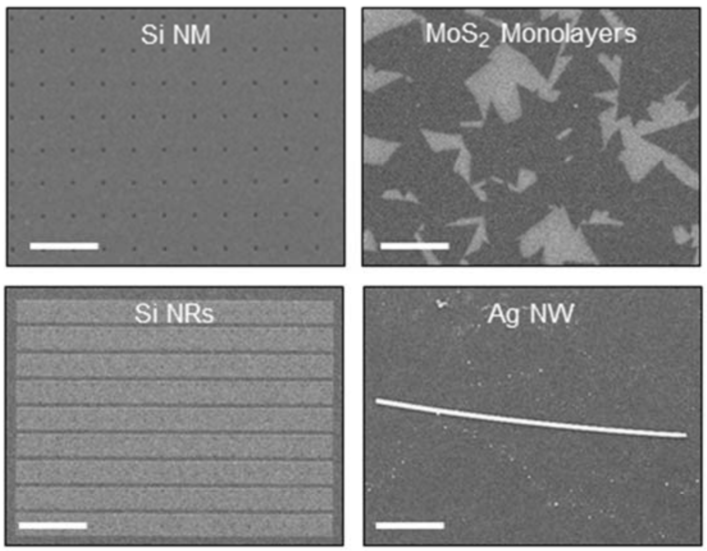

Fig. S1

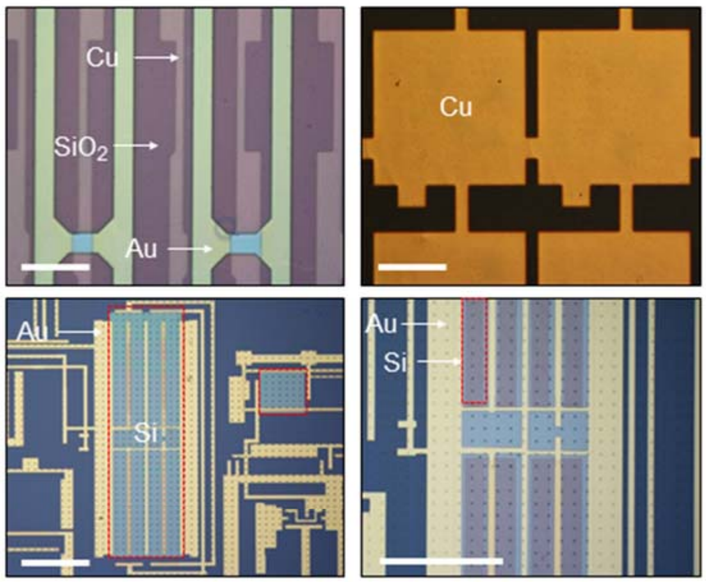

Fig. S2

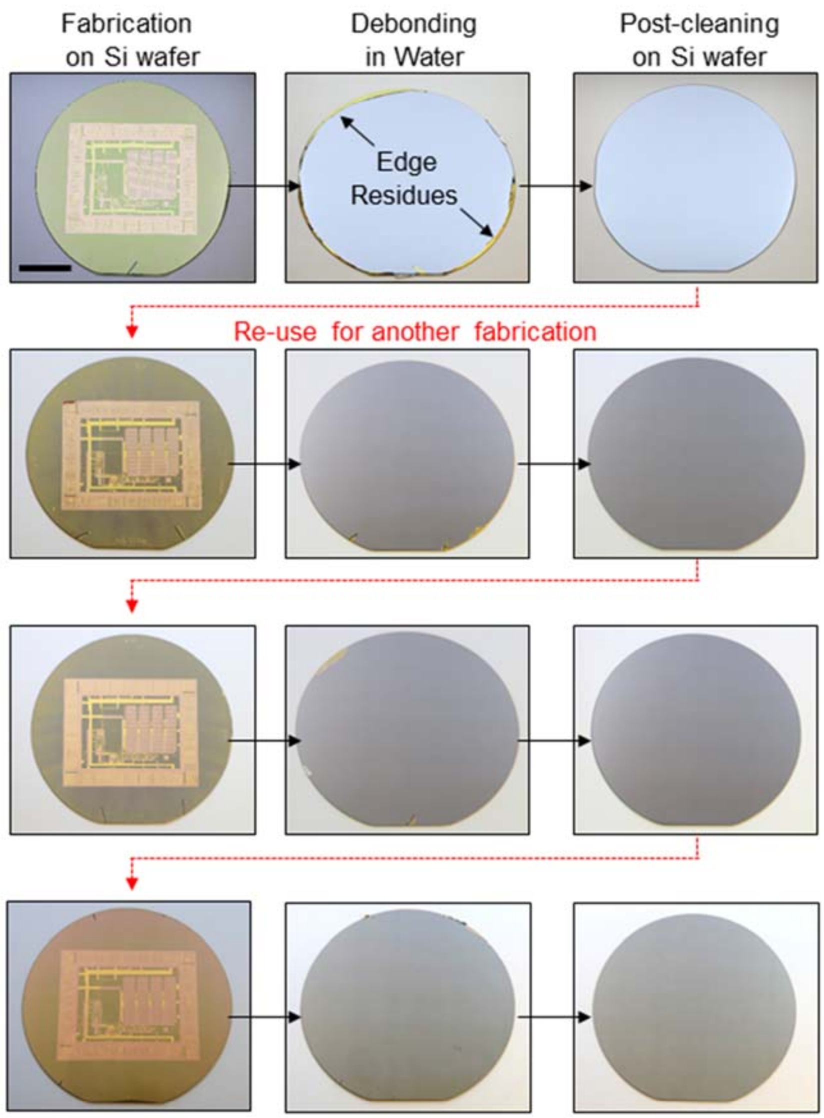
Fabrication
on Si wafer
Debonding
in Water
Post-cleaning
on Si wafer
Edge
Residues
Re-use for another fabrication

Fig. S3

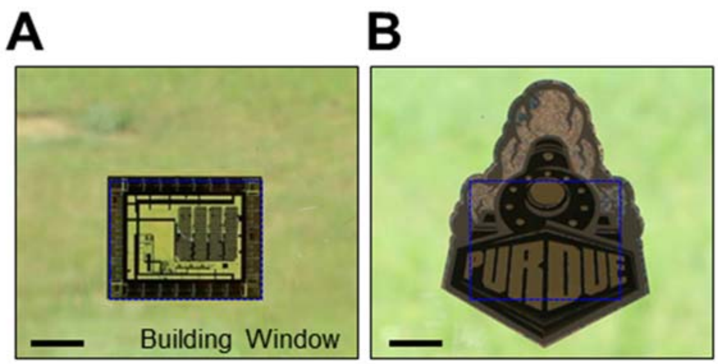

Fig. S4

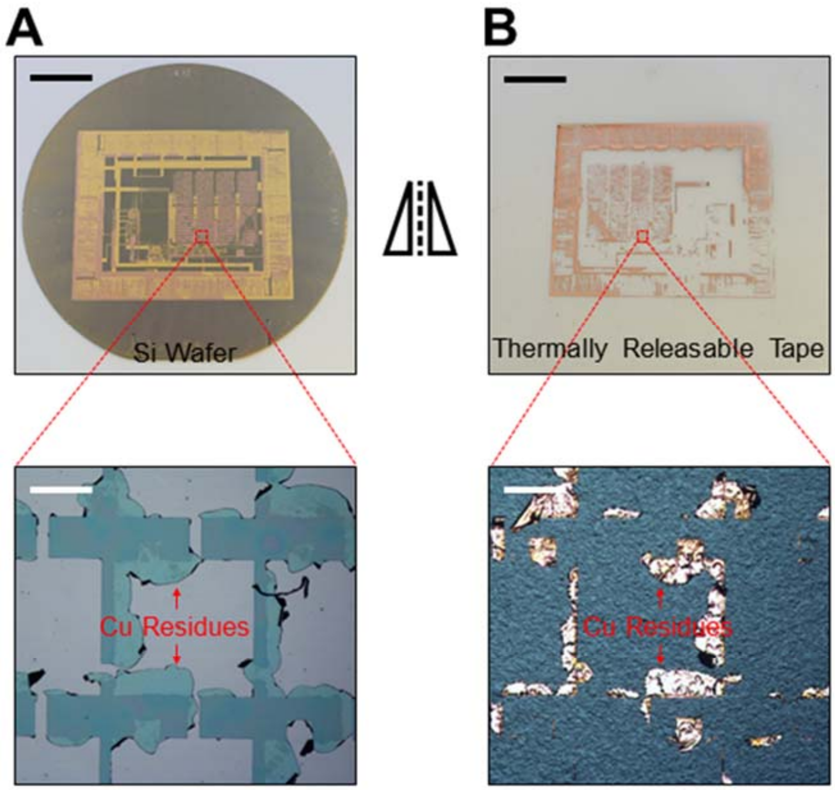
A
B
Si Wafer
Thermally Releasable Tape
Cu Residues
Cu Residues

Fig. S5

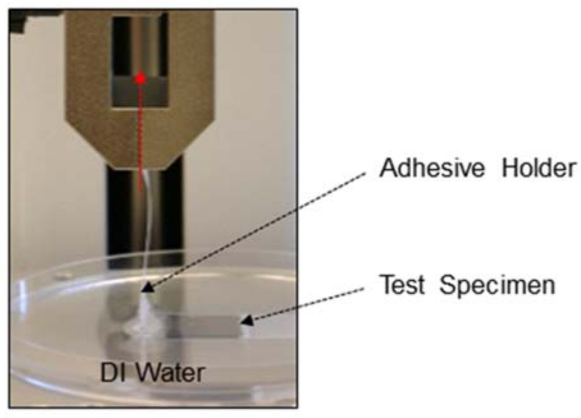

Fig. S6

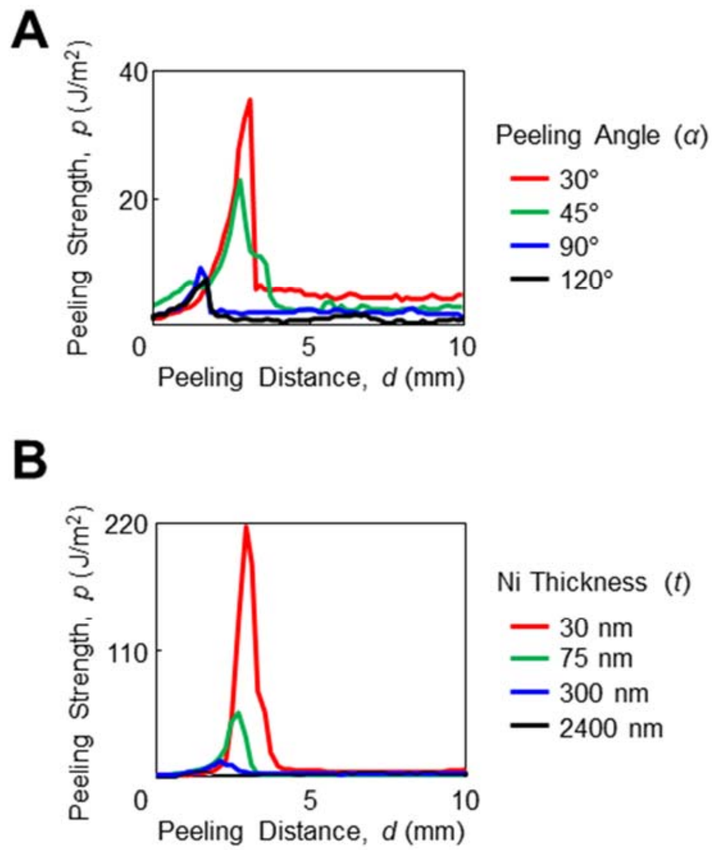
A
Peeling Strength, p (J/m2)
40
20
0
5
10
Peeling Distance, d (mm)
Peeling Angle (α)
30°
45°
90°
120°
B
Peeling Strength, p (J/m2)
220
110
0
5
10
Peeling Distance, d (mm)
Ni Thickness (t)
30 nm
75 nm
300 nm
2400 nm

Fig. S7

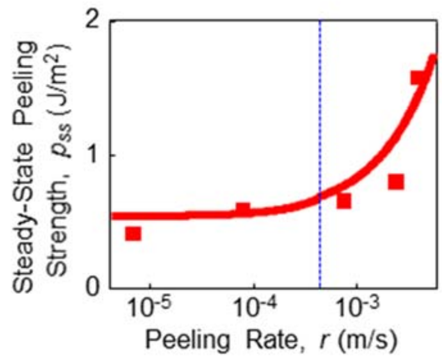
2
1
0
Steady-State Peeling Strength, p_{ss} (J/m^2)
10^{-5}
10^{-4}
10^{-3}
Peeling Rate, r (m/s)

Fig. S8

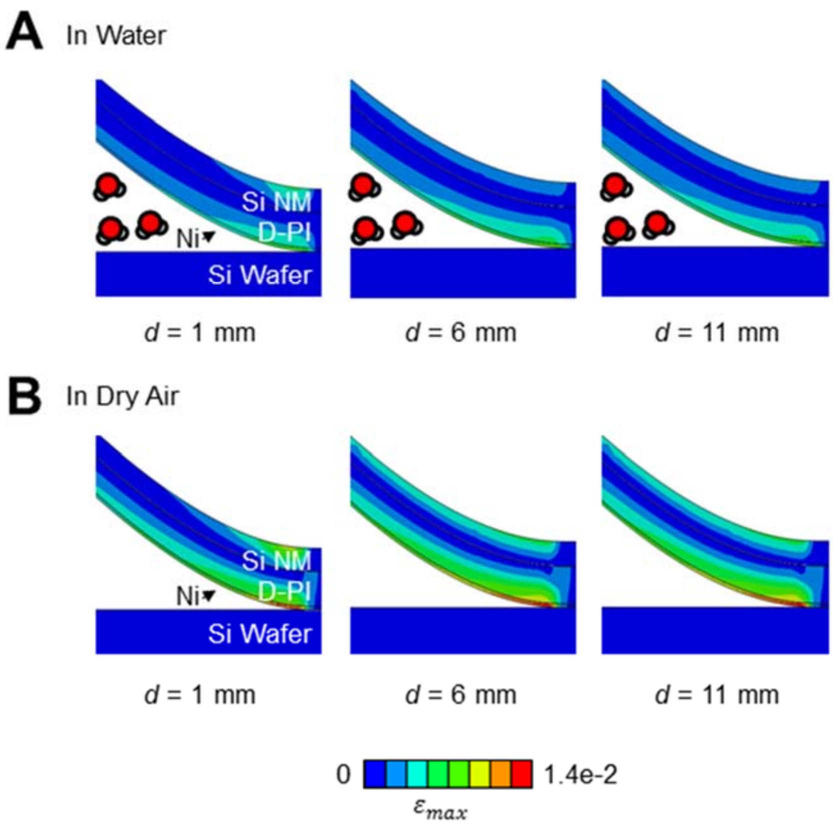
A
In Water
Si NM
D-PI
Ni
Si Wafer
d = 1 mm
d = 6 mm
d = 11 mm
B
In Dry Air
Si NM
D-PI
Ni
Si Wafer
d = 1 mm
d = 6 mm
d = 11 mm
0
1.4e-2
ε_{max}

Fig. S9

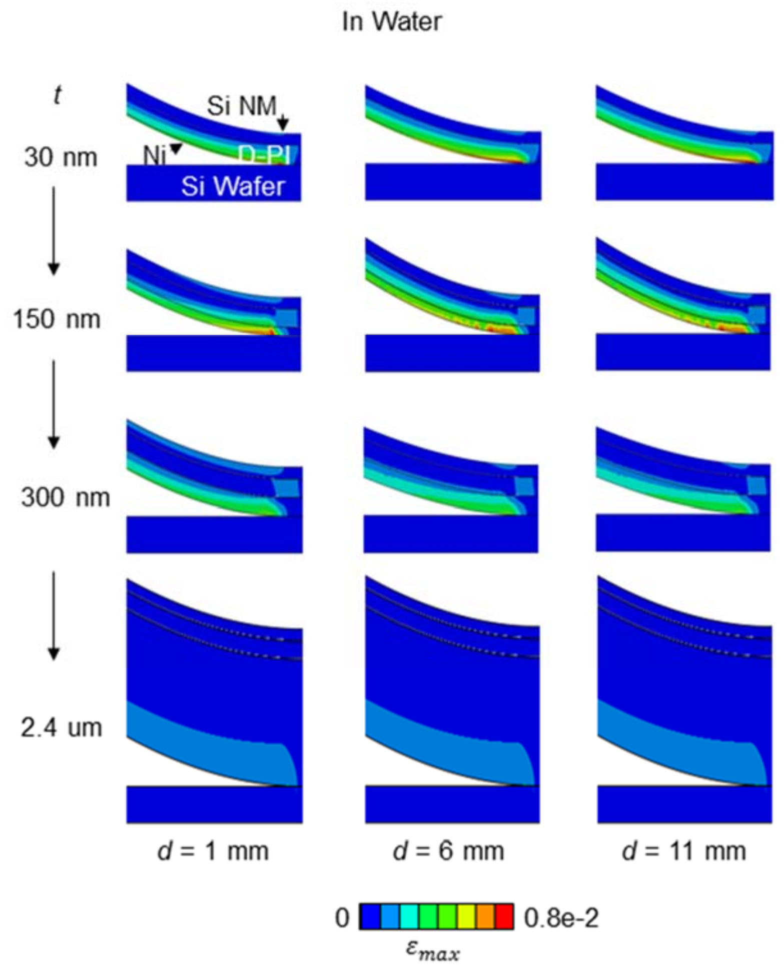
In Water
t
Si NM
Ni
D-PI
Si Wafer
30 nm
150 nm
300 nm
2.4 um
d = 1 mm
d = 6 mm
d = 11 mm
0
0.8e-2
ε_{max}

Fig. S10

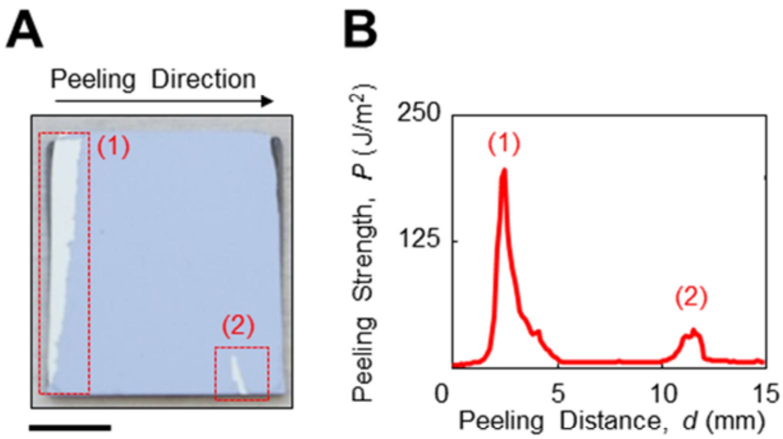
A
Peeling Direction
(1)
(2)
B
250
125
0
5
10
15
Peeling Strength, P (J/m2)
Peeling Distance, d (mm)
(1)
(2)

Fig. S11

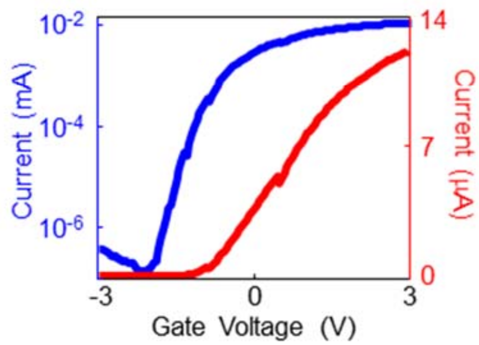

Fig. S12

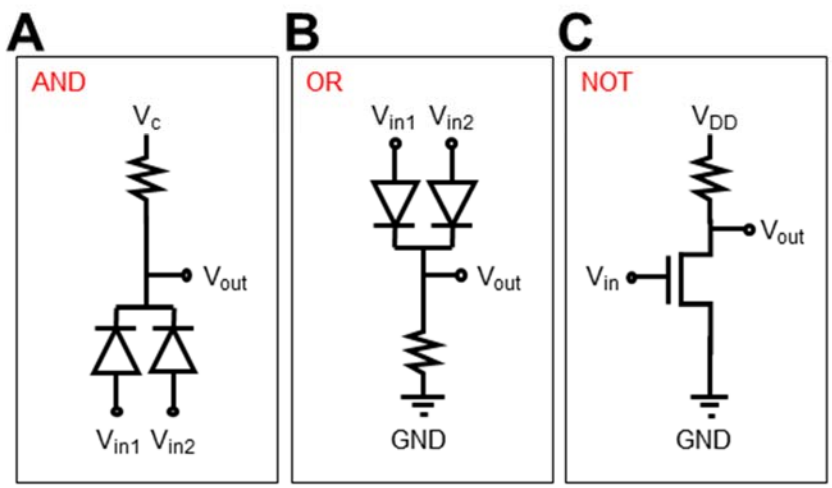
A
AND
Vc
Vout
Vin1 Vin2
B
OR
Vin1 Vin2
Vout
GND
C
NOT
VDD
Vout
Vin
GND

Fig. S13

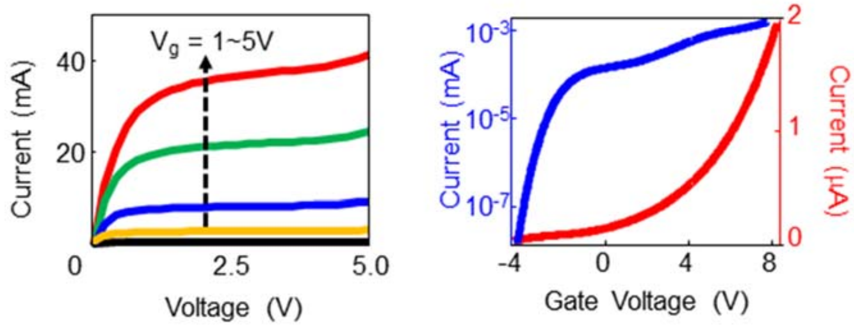

V_g = 1~5V
Current (mA)
40
20
0
2.5
5.0
Voltage (V)
10^-3
10^-5
10^-7
Current (mA)
2
1
0
Current (µA)
-4
0
4
8
Gate Voltage (V)

Fig. S14

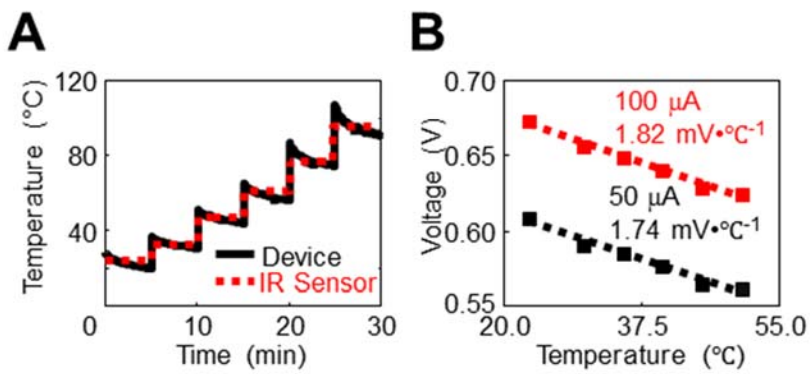
A
Temperature (°C)
120
80
40
0
10
20
30
Time (min)
Device
IR Sensor
B
Voltage (V)
0.70
0.65
0.60
0.55
20.0
37.5
55.0
Temperature (°C)
100 μA
1.82 mV•°C-1
50 μA
1.74 mV•°C-1

Fig. S15

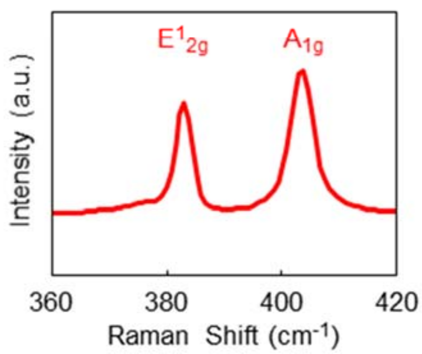

Fig. S16

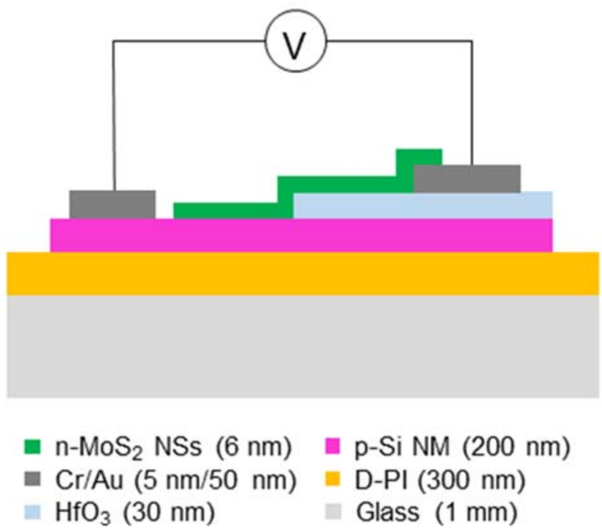
V
n-MoS2 NSs (6 nm)
p-Si NM (200 nm)
Cr/Au (5 nm/50 nm)
D-PI (300 nm)
HfO3 (30 nm)
Glass (1 mm)

Fig. S17

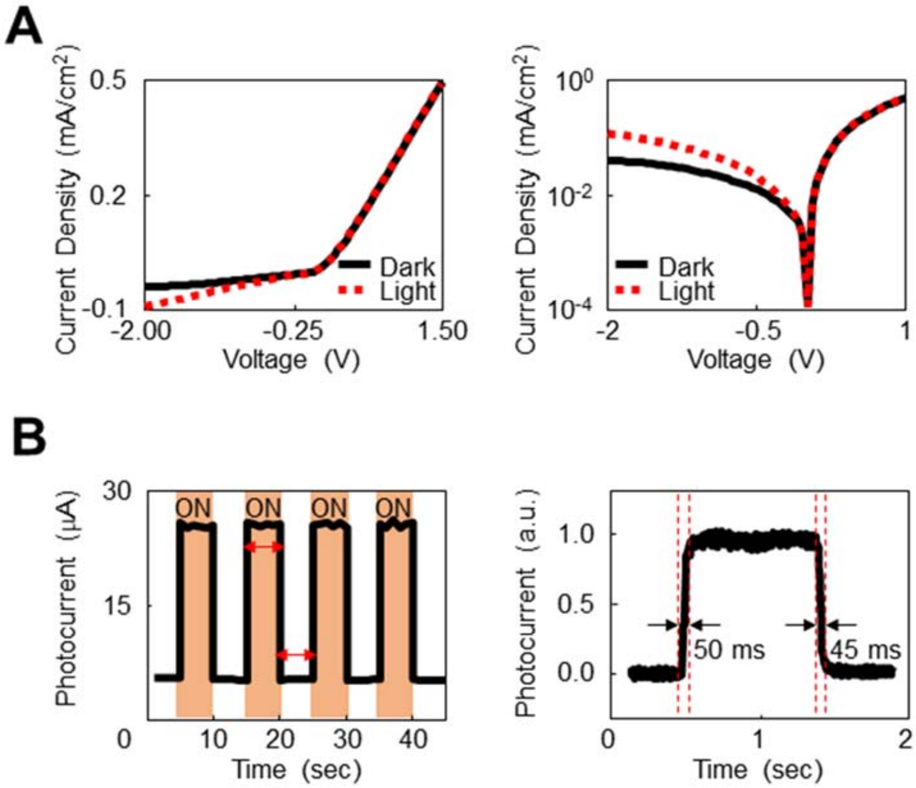
A
Current Density (mA/cm^2)
0.5
0.2
-0.1
-2.00
-0.25
1.50
Voltage (V)
Dark
Light
Current Density (mA/cm^2)
10^0
10^{-2}
10^{-4}
-2
-0.5
1
Voltage (V)
Dark
Light
B
Photocurrent (μA)
30
15
0
10
20
30
40
ON
ON
ON
ON
Time (sec)
Photocurrent (a.u.)
1.0
0.5
0.0
0
1
2
50 ms
45 ms
Time (sec)

Fig. S18

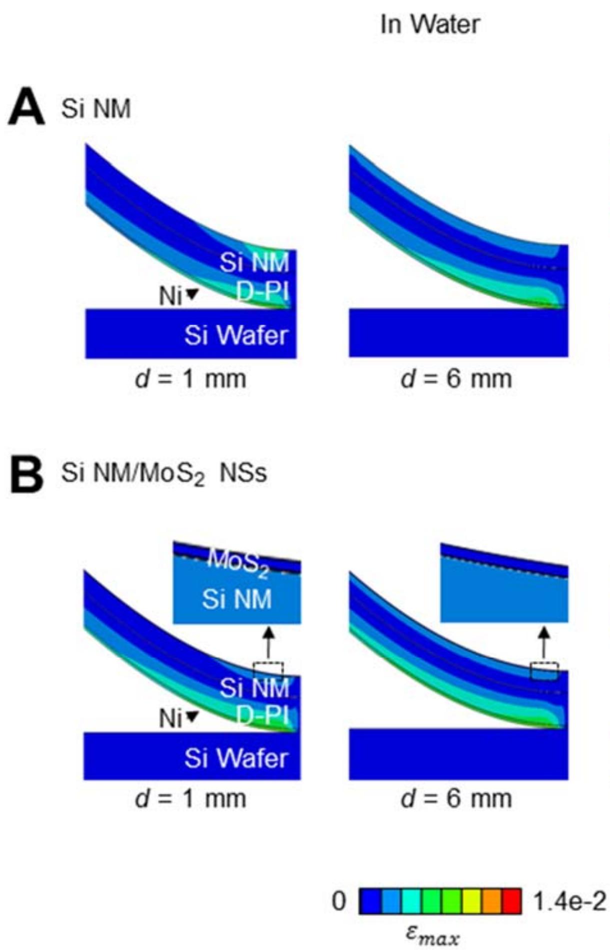
In Water
A
Si NM
Si NM
Ni
D-PI
Si Wafer
d = 1 mm
d = 6 mm
d = 11 mm
B
Si NM/MoS2 NSs
MoS2
Si NM
Si NM
Ni
D-PI
Si Wafer
d = 1 mm
d = 6 mm
d = 11 mm
0
1.4e-2
ε_max

Fig. S19

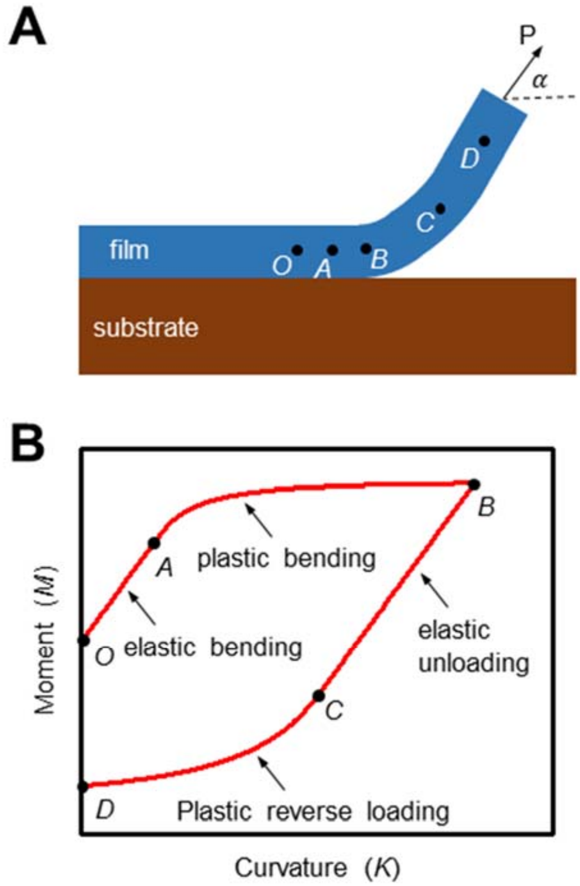
A
P
α
D
C
film
O
A
B
substrate
B
B
plastic bending
A
Moment (M)
O
elastic bending
elastic
unloading
C
D
Plastic reverse loading
Curvature (K)

Fig. S20